Frontiers in Bioscience Landmark

Front. Biosci. (Landmark Ed) **2024**; 29(3): 91
https://doi.org/10.31083/j.fbl2903091

Original Research

Bioinformatics-Based Screening of Key LncRNAs for Modulating the Transcriptome Associated with Glaucoma in Human Trabecular Meshwork Cells

Junhong Guo[1], Yunfei Wu[2], Yue Sun[2], Dong Chen[2], Yijia Huang[1], Xiaoli Shen[1], Zhichao Yan[1,*], Jiantao Wang[1,*]

[1]Shenzhen Eye Hospital, Jinan University, Shenzhen Eye Institute, 518040 Shenzhen, Guangdong, China
[2]Center for Genome Analysis, Ruixing Biotechnology Co., Ltd., 430075 Wuhan, Hubei, China
*Correspondence: tiaosuper@163.com (Zhichao Yan); wangjiantao65@126.com (Jiantao Wang)
Academic Editor: Ilaria Baglivo
Submitted: 17 September 2023 Revised: 23 November 2023 Accepted: 12 December 2023 Published: 29 February 2024

Abstract

Objective: The morphology and functions of the human trabecular meshwork (HTM) are dysregulated in glaucoma, and the molecular mechanisms of this dysregulation remain unknown. According to an established *in vitro* model, whose function was to study the regulatory networks sustaining the response of HTM cells to the increased substrate stiffness, we systematically analyzed the expression pattern of long noncoding RNAs (lncRNAs), the important regulatory RNAs in cells. **Methods**: Bioinformatics analysis was performed to identify the dysregulated lncRNAs in response to increased substrate stiffness using transcriptome sequencing data (RNA-seq). Then we interfered with the expression of several dysregulated lncRNAs in HTM cells to explore their molecular targets. The cross-linking immunoprecipitation and sequencing method (CLIP-seq) was used to identify enhancer of zeste homolog 2 (EZH2)-targeted RNAs in HTM cells. The chromatin IP and sequencing method (ChIP-seq) was used to identify the targets of EZH2 and histone H3 at lysine 27 (H3K27me3). **Results**: The response of thousands of dysregulated lncRNAs to increased substrate stiffness was identified through RNA-seq. Functional prediction of these lncRNAs revealed that they potentially regulated key biological processes, including extracellular matrix (ECM) organization. By interfering with the expression of lncRNA *SHNG8*, *ZFHX4-AS1*, and *RP11-552M11.4*, the results demonstrated that those lncRNAs extensively regulated the expression levels of ECM-associated genes. Moreover, we found that EZH2 expression was significantly decreased at high substrate stiffness. Using CLIP-seq to identify EZH2-targeted RNAs in HTM cells, we found that SNHG8 was bound by EZH2. According to the CLIP-seq data of EZH2, we found that EZH2 binding sites were observed in the transcripts of SNHG8-regulated genes, but not in the ChIP-seq results of EZH2 and H3K27me3. **Conclusion**: Our results suggest that SNHG8 and EZH2 may cooperate to regulate the expression of a subset of genes by influencing their RNA abundance, explaining how they support HTM cell morphology and high density. This study contributes to the understanding of the alteration of HTM during the progression of glaucoma by identifying functional lncRNAs, especially SNHG8, and suggests novel therapeutic targets to treat glaucoma.

Keywords: glaucoma; human trabecular meshwork cells; lncRNAs; EZH2; SNHG8

1. Introduction

Glaucoma is the leading cause of irreversible blindness worldwide, with elevated intraocular pressure (IOP) being the major risk factor, especially for primary open-angle glaucoma (POAG) [1,2]. Short-term IOP fluctuation is a signature risk of glaucoma [3]. Thus, IOP has been considered a therapeutic target by modulating its level in glaucoma patients [4]. At the molecular level, several molecules reportedly elevate IOP in glaucoma, including FN-EDA/TLR4 axis [5], Src/TGF-β axis [6], and eNOS [7]. At the cellular level, human trabecular meshwork (HTM) cells function normally under persistent mechanical stress which is a key regulator of IOP [8]. Fluorescent cell membrane probes have shown that the corneoscleral and JCT meshwork have a higher density of HTM cells than the uveal meshwork [9]. The extracellular matrix (ECM) synthesized by HTM cells also play important roles in the homeostasis of IOP via its remodeling [10–12]. However, how HTM responds to cyclic IOP fluctuation and how this dysregulation develops into glaucoma should be further investigated.

An *in vitro* HTM cellular model simulating the *in vivo* HTM cell environment is necessary to investigate the underlying mechanisms of increased IOP in glaucoma patients. A previous study demonstrated that HTM cells cultured on polyacrylamide hydrogels with altered compliance values can mimic the *in vivo* glaucomatous HTM cells [13]. High meshwork compliance mimicking glaucoma can affect HTM cell physiology and subsequent responses. Alterations in substratum compliance simulating the glaucoma-related environment can also regulate the compliance of HTM cells [14]. Our previous study also demonstrated the highly dynamic expression patterns of protein-coding genes and noncoding RNAs of HTM cells by changing the poly-

acrylamide hydrogel stiffness, and validated ECM gene expression changes using clinical HTM tissues [15,16]. However, how those HTM cells respond to normal IOP fluctuation and mechanical stresses, and when HTM cells become dysfunctional under overload substratum stiffness are unknown.

In ophthalmology, the high-throughput sequencing method has been employed to explore disease biomarkers [17]. Meanwhile, long noncoding RNAs (lncRNAs) also participate in the pathogenesis of glaucoma on a genetic basis [18,19]. In rats with glaucoma, lncRNA-*MALAT1* mediates neurodegeneration through the continuous CREB signaling activation [20]. However, most studies on the role of lncRNAs in glaucoma have focused on the genetic variation [21]. LncRNAs can perform their functions with diverse mechanisms, including their primarily studied function of cis/trans-acting transcriptional regulation helped by other proteins, such as polycomb repressive complex 2 (PRC2) [22,23]. Thus, the underlying mechanisms of lncRNAs in glaucoma need to be further investigated.

According to our previously established *in vitro* HTM cell model mimicking *in vivo* IOP increasing in glaucoma and high-throughput transcriptome sequencing (RNA-seq) data [15], we investigated the dysregulation of lncRNAs under high substratum compliance and predicted their potential targets. Additionally, we selected several highly dysregulated lncRNAs and altered their expression levels to validate their downstream targets using the RNA-seq method. Our study provides insights into how lncRNA expression profiles are dysregulated in pressure-increasing HTM cells and reveals the complicated lncRNA-mRNA regulatory mechanisms.

2. Materials and Methods

2.1 LncRNA Cloning and Plasmid Construction

The human *SNHG8*, *ZFHX4-AS1* and *RP11-552M11.4* genes were cloned by reverse transcription and polymerase chain reaction (PCR) amplification methods. The purified DNA fragment from a gel (28004, MinElute PCR Purification Kit, Qiagen, MD, USA) was cloned into the pIRES-hrGFP-1a vector (240031, Agilent Technologies, Savage, MD, USA) using the hot fusion method by CE Design V1.04 (Vazyme Biotech Co., Ltd., Nanjing, China). Plasmids were introduced into *Escherichia coli* strain by chemical transformation. Then *E. coli* strains were plated onto LB agar plates with 1 µL/mL ampicillin (7177-48-2; Sigma, St. Louis, MO, USA), and incubated overnight at 37 °C. Colony PCR (28 cycles) was used to screen lncRNA colonies with universal primers (located on the backbone vector). Finally, the inserted sequences of lncRNAs were verified by Sanger sequencing.

2.2 Cell Culture and Transfections

Primary HTM cells (YS905C, Yaji Biological, Shanghai, China) were donated by anonymous deceased individuals without detailed information, cultured in DMEM/F12 (PM150310, Procell, Wuhan, China), and were validated by STR profiling, and tested negative for mycoplasma. Cells were cultured in a humidified incubator at 37 °C and 5% CO_2. Plasmid transfection was performed with Lipofectamine 2000 (Invitrogen, Carlsbad, CA, USA). For the *in vitro* stiffness model, HTM cells were cultured on polyacrylamide hydrogel with gradually increased bisacrylamide concentrations (0.04%, 0.1%, 0.2%, 0.5%, 1.3%, and 2.08%), mimicking the increased Young's modulus (1.1, 2.5, 4.2, 11.9, 34.4, and 50 kPa) [15,24]. For lncRNA plasmid transfection and enhancer of zeste homolog 2 (EZH2) immunoprecipitation experiments, HTM cells were treated under normal conditions.

2.3 Gene Expression Assessment (Reverse Transcription and Quantitative Polymerase Chain Reaction, RT-qPCR)

We used glyceraldehyde-3-phosphate dehydrogenase (*GAPDH*) as an internal control for assessing the effects of *SNHG8*, *ZFHX4-AS1*, and *RP11-552M11.4* overexpression, as well as the ECM-related gene expression. The cDNA synthesis and following RT-qPCR were performed on the Bio-Rad S1000 Thermal Cycler with Hieff™ qPCR SYBR® Green Master Mix (Low Rox Plus; YEASEN, Shanghai, China), followed by denaturing at 95 °C for 10 min, 40 cycles of denaturing at 95 °C for 15 sec and annealing and extension at 60 °C for 1 min. The expression level of each transcript was normalized to *GAPDH* by the $2^{-\Delta\Delta CT}$ method [25] using three technical replicates. The detailed sequences of primers are presented in **Supplementary Table 1**.

2.4 Ultraviolet Cross-Linking and Immunoprecipitation

HTM cells were prepared for ultraviolet (UV) cross-linking with UV irradiation type C (254 nm) at 400 mJ per cm^2. Cross-linked cell lysis was performed with 1% RNase inhibitor (2313u, Takara, Beijing, China) and a 2% protease inhibitor cocktail (B14001, Bimake, Shanghai, China) for 30 min. RQ1 DNase (M6101, Promega, Madison, WI, USA) was added to the lysate to digest the DNA. Then RNA was digested by adding micrococcal nuclease (88216, Thermo Fisher Scientific, Waltham, MA, USA). For IP, cell lysate was incubated with 15 µg anti-EZH2 antibody (5246, Cell Signaling Technology, Danvers, MA, USA) or control IgG antibody (12-371, Millipore, Burlington, MA, USA) overnight at 4 °C with two biological replicates. The immunoprecipitated protein-RNA complexes were eluted and isolated from the gel. Then the recovered RNA was prepared for library preparation using kit for small/microRNA (K02420-L, Gnomegen, San Diego, CA, USA). The libraries were applied to the Illumina HiSeq X Ten system for 150 nucleotide (nt) paired-end sequencing.

2.5 Chromatin Immunoprecipitation-Sequencing (ChIP-seq)

HTM cells were cross-linked with 1% formaldehyde for 10 min at room temperature and then lysed to obtain a chromatin-protein complex. Soluble sheared chromatin was obtained by sonication (average DNA length of 200–500 base pairs). The 10 µg anti-EZH2 antibody (5246, Cell Signaling Technology, Boston, MA, USA) and anti-H3K27me3 antibody (12-565, Millipore, Burlington, MA, USA) were used for IP with 100 µL chromatin as input at 4 °C overnight with two biological replicates. The next day, 30 µL protein beads were added and the samples were further incubated for 3 h. Immunoprecipitated DNA was used to construct the sequencing libraries following the protocol of ChIP-seq Library Prep Kit (NOVA-5143-02, Bioo Scientific, Austin, TX, USA) and the libraries were applied to the Illumina HiSeq X Ten system (Illumina, Inc., San Diego, CA, USA) for 150 nt paired-end sequencing.

2.6 Retrieval and Process of RNA-seq Data

The RNA-seq data files of GSE123100 from our previous study [15] were re-analyzed. The raw files were converted to fastq file by the National Center for Biotechnology Information (NCBI) Sequence Read Archive (SRA) Tool fastq-dump. Low-quality bases were removed from the raw reads using the FASTX-Toolkit (version 0.0.13, The Hannon Lab, New York, NY, USA; http://hannonlab.cshl.edu/fastx_toolkit/). The short reads less than 16 nt were also dropped. Then the quality filtered reads were evaluated using FastQC (version0.12.1, Babraham Institute, Cambridge, MA, USA, http://www.bioinformatics.babraham.ac.uk/projects/fastqc).

2.7 Raw Data Filtering and Alignment

Raw sequenced reads were filtered to remove low quality reads using the above methods. Then, clean reads were aligned onto the human GRCH38 genome using the HISAT2 (version2.2.1, University of Texas Southwestern Medical Center, Dallas, TX, USA) alignment program [26] with no more than four mismatches. Uniquely mapped reads were used for gene expression calculation by FPKM values (fragments per kilobase of transcript per million fragments mapped) [27]. The statistical power of this experimental design (one biological replicates), calculated by online implementation (https://rodrigo-arcoverde.shinyapps.io/rnaseq_power_calc/) was 0.93.

2.8 Novel Transcript Assembly and LncRNA Prediction

StringTie (version2.1.6, Johns Hopkins University, Baltimore, MD, USA) [28] was used to assemble and predict transcripts. Final transcripts were screen out by eliminating the transcripts with FPKM <1, and then were combined into one general transfer format (GTF) file. We then used four software to predict coding potential of transcripts: CPC2 (version2.0, Peking University, Beijing, China) [29], LGC (version1.0, Chinese Academy of Sciences, Beijing, China) [30], CNCI (version2.0, Chinese Academy of Sciences, Beijing, China) [31] and CPAT (version3.4.0, Mayo Clinic College of Medicine, Houston, TX, USA) [32]. The filtering steps for lncRNA selection were followed one published study [33]. Briefly, Transcripts without coding potential, longer than 200 nt, and more than 1000 bp distance from the adjacent coding genes, were considered lncRNAs.

2.9 Differentially Expressed Genes (DEG) Analysis

We used edgeR (version3.32, The Walter and Eliza Hall Institute of Medical Research, Parkville, Victoria, Australia) [34] to identify DEGs with p-value < 0.01 and fold change >1.5 (up) or <0.67 (down) as the cut-off criteria according to our previous study using the same dataset [15]. Another reason for this threshold was the small amplitude of transcriptome alternation caused by the increased stiffness.

2.10 Cross-Linking Immunoprecipitation and Sequencing (CLIP-seq) and ChIP-seq Data Analyses

After alignment, uniquely mapped reads were used to predict EZH2-bound regions (peaks) by the "ABLIRC" strategy (version1.0, ABLife Inc., Wuhan, China) [35] and CIMS (version1.0, The Rockefeller University, New York, NY, USA) [36]. After stimulation and calculation, all the observed peaks with p-value < 0.05 were selected. For ChIP-seq, reads were aligned to the reference using Bowtie2 (version2.4.4, University of Maryland, College Park, MD, USA) with one mismatch [37]. ChIP-seq peak calling was performed using MACS14 (version1.4.2, Dana-Farber Cancer Institute and Harvard School of Public Health, Boston, MA, USA) with default settings and p-value $< 1 \times 10^{-5}$ [38]. The binding motifs of EZH2 protein were identified using HOMER software (version3.12, University of California, San Diego, CA, USA) [39] with the default setting.

2.11 Functional Enrichment and Other Statistical Analysis

Gene Ontology (GO) and Kyoto Encyclopedia of Genes and Genomes (KEGG) pathways were identified to sort out the functional categories of DEGs with the KOBAS server (version2.0, Peking University, Beijing, China) [40]. Principal component analysis (PCA) was performed using R package factoextra (https://cloud.r-project.org/package=factoextra). The pheatmap package (https://cran.r-project.org/web/packages/pheatmap/index.html) in R software (version4.2, https://www.r-project.org) was used to perform clustering based on Euclidean distance. Student's t-test was used to compare the two groups with p-value < 0.05 considered statistically significant. The Pearson's correlation coefficient (PCC) was used to calculate the correlation between differentially expressed lncRNAs (DElncRs) and DEGs; p-value < 0.01 and absolute PCC >0.9 were used as the criteria. Venn diagram and associated hypergeometric test were performed in R software (version 4.2).

3. Results

3.1 Global Identification and Expression Pattern Analysis of LncRNAs in HTM Cells

Our previous study systematically investigated the mRNA expression profiles in response to the tunable stiffness and found extensive dysregulation of ECM-associated genes [15]. Here, we explored the expression profile of lncRNAs, which are important regulatory RNAs that may influence the global transcriptome profile. We re-analyzed the GSE123100 dataset and performed lncRNA prediction and expression analyses. The investigation pipeline used in this study is shown in Fig. 1A. Biological replicates were HTM cells cultured for 3 days (D3) and 5 days (D5) with the same Young's modulus. After predicting novel lncRNAs and calculating their expression levels, we divided the expressed genes into mRNA and lncRNA groups. The PCA results demonstrated that D3 and D5 samples were separated by the first component, and that obvious distances for D5 samples with high Young's modulus were observed (Fig. 1B). Then we assessed the expression patterns of several glaucoma-associated lncRNAs, including *ANRIL*/*CDKN2B-AS1*, *MALAT1*, and *LOXL1-AS1* [18]. *ANRIL*/*CDKN2B-AS1* showed lower expression levels at 1.1 kPa and 50 kPa; the expression level of *LOXL1-AS1* was decreased at 50 kPa; whereas *MALAT1* showed specifically higher expression level at 50 kPa (Fig. 1C). These results demonstrated that their expression patterns were dynamically changed with the increase of Young's modulus. Together, these results indicated that in HTM cells, lncRNA expression levels are extensively regulated by increased substrate stiffness and that lncRNAs may have important regulatory functions. We then analyzed the differentially expressed lncRNAs (DElncRs) using the same method for mRNAs [15]. By analyzing DElncRs between adjacent samples with increased stress, we found that DElncR number was the largest in 34.3 kPa *vs.* 11.9 kPa, following by 11.9 kPa *vs.* 2.5 kPa, and that DelncR number was very small in samples with lowest or highest stress (Fig. 1D). According to a previous study, the average Young's modulus of HTM was 80.0 $\pm$ 32.5 kPa in glaucomatous tissue [41], consistent with our discovery that the largest DElncR number was detected in the 34.3 kPa *vs.* 11.9 kPa group. The PCA result demonstrated the high discreteness of all of the DElncRs (Fig. 1E), suggesting that the expression patterns of lncRNAs vary with the increased stiffness.

3.2 Dysregulated LncRNAs by Tunable Stiffness are Associated with the ECM Organization of HTM Cells

Based on the above results, we explored the potential functions of DElncRs in HTM cells. Focusing on the two groups with the most DElncRs (Fig. 1D), we found that 97 DElncRs were detected in both groups (Fig. 2A, p-value = 3.43347×10^{-50}, hypergeometric test). Then we analyzed the potential functions of these shared DElncRs by co-expression analysis with the identified DEGs. After the co-expressed DElncR-DEG pairs were filtered with correlation coefficient >0.9 and p-value < 0.01, 1621 and 4031 pairs were detected from the 11.9 kPa *vs.* 2.5 kPa and 34.4 kPa *vs.* 11.9 kPa groups, respectively. Then, we performed functional enrichment analyses of these co-expressed DEGs. From the 11.9 kPa *vs.* 2.5 kPa group, the immune response and cytokine-mediated signaling pathways were enriched (Fig. 2B). From the 34.4 kPa *vs.* 11.9 kPa group, co-expressed DEGs were significantly enriched in response to mechanical stimulus, negative regulation of chondrocyte differentiation, and integrin-mediated signaling pathways; ECM organization was also enriched (Fig. 2C). The cellular component of these co-expressed DEGs also revealed their enrichment in ECM-related pathways (**Supplementary Fig. 1A,B**). Fig. 2A shows the co-expressed DEGs of overlapped DElncRs. Although insignificant, the extracellular space and extracellular region were the top two cellular components (**Supplementary Fig. 1C**). These results indicate that DElncRs may regulate the expression of ECM-related genes and participate in the pathogenesis of glaucoma. To have a closer view of the DElncRs and their co-expressed DEGs, we plotted the potentially regulatory network between DElncRs and DEGs derived from ECM-related pathways (Fig. 2D). Heatmap analysis of DElncRs associated with ECM-related pathways revealed that they were highly dysregulated due to the increased substrate stiffness (Fig. 2E).

According to these results, we proposed that lncRNA expression levels were extensively changed between 11.9 kPa *vs.* 34.4 kPa, and were associated with ECM organization. Next, we selected several lncRNA-mRNA pairs with a negative correlation to further explore their relationships. The following 10 lncRNAs were selected to explore their potential functions: *ZFHX4-AS1*, *NNF-AS1*, *CRNDE*, *TP73-AS1*, *SNHG8*, *DLEU2*, *CTD-3252C9.4*, *LINC00707*, *RP11-552M11.4*, and *MEG8*. Most of these lncRNAs were located in intergenic regions, and may regulate other genes or RNAs in a cis or trans manner. Three lncRNAs, *ZFHX4-AS1*, *NNF-AS1*, and *TP73-AS1*, were at the antisense strand of protein coding genes, functioning in a cis manner. These known lncRNAs were classified into two clusters: increased expression levels by elevated stiffness, and the contrary cluster. The RT-qPCR experiment was performed to validate their expression patterns during substrate stiffness elevation. The RT-qPCR results of the eight lncRNAs showed a consistent pattern with the RNA-seq data (Fig. 3, **Supplementary Table 1**). These results demonstrated that the dysregulated lncRNAs may have important functions in the HTM cells of glaucoma pathogenesis.

3.3 Overexpression of Selected LncRNAs Extensively Regulates the ECM Gene Expression of HTM Cells

To further explore the functions of these selected lncRNAs, we attempted to construct lncRNA overexpression cell models by transfecting overexpression plasmids into

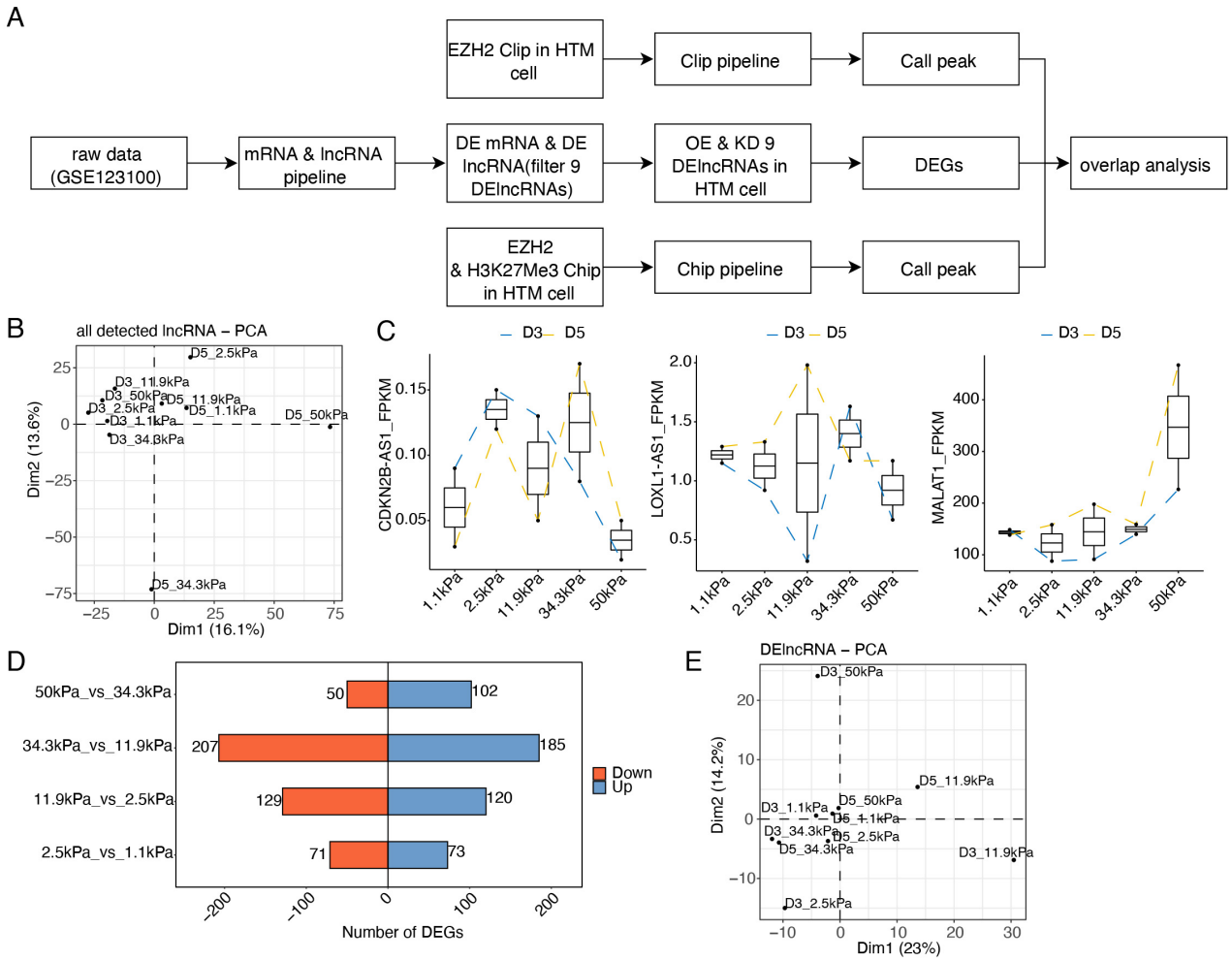

Fig. 1. Global analysis of long noncoding RNAs (lncRNAs) from human trabecular meshwork (HTM) cells. (A) The work flow of this study. (B) Principal component analysis (PCA) results showing the diversity of expressed lncRNAs in the HTM cell model. (C) Line plot showing the expression patterns of CDKN2B-AS1, MALAT1, and LOXL1-AS1 in HTM cells in response to stiffness. (D) Bar plot showing the numbers of differentially expressed lncRNAs (DElncRs) in different groups. (E) PCA result showing the diversity of DElncRs in the HTM cell model. mRNA, messenger RNA; CLIP, cross-linking immunoprecipitation; EZH2, enhancer of zeste homolog 2; DE, differentially expressed; Chip, chromatin immunoprecipitation; DEGs, differentially expressed genes; OE, over expression.

normal HTM cells. Plasmid without lncRNA sequences was used as the common negative control (NC). RT-qPCR has validated the overexpressed transcriptional levels of several lncRNAs (Fig. 4A). Finally, three lncRNAs with significant expression changes were selected for overexpression experiments, including *ZFHX4-AS1*, *SNHG8*, and *RP11-552M11.4*. Meanwhile, *ZFHX4-AS1* itself had control (NC_ZFHX4-AS1_OE) because the experiment was done in another batch, and SNHG8 and *RP11-552M11.4* had the same control (NC_OE). Then RNA-seq experiments were performed to explore the transcriptional influence of these three lncRNAs. The expression analyses showed that they showed distinct higher levels in the corresponding overexpression samples, and were not changed in other samples (Fig. 4B). Sample correlation analysis revealed that overall gene expression levels were highly correlated with PCCs $\geq$0.98 except the NC_ZFHX4-AS1_OE sample (Fig. 4C). These results indicated that lncRNA dysregulation did not trigger overall transcriptional alternation. The EdgeR [34] method was employed to perform DEG analysis with false discovery rate (FDR) $<$0.05 and fold change (FC) $>$2. The DEG number between lncRNA overexpression *vs.* NC group ranged from 296 to 749 (Fig. 4D), accounting for 1–3% of total detected genes. We then performed functional enrichment analyses of these DEGs. Extracellular space- and extracellular region-related cellular component terms were significantly enriched in both the up- and down-regulated genes (Fig. 4E–G). The DEGs involved in ECM were regulated by these lncRNAs. *ZFHX4-AS1* especially increased the expression levels of 24 ECM-related genes, and decreased the expression levels of 46 genes, thus having the most significant influence. Next,

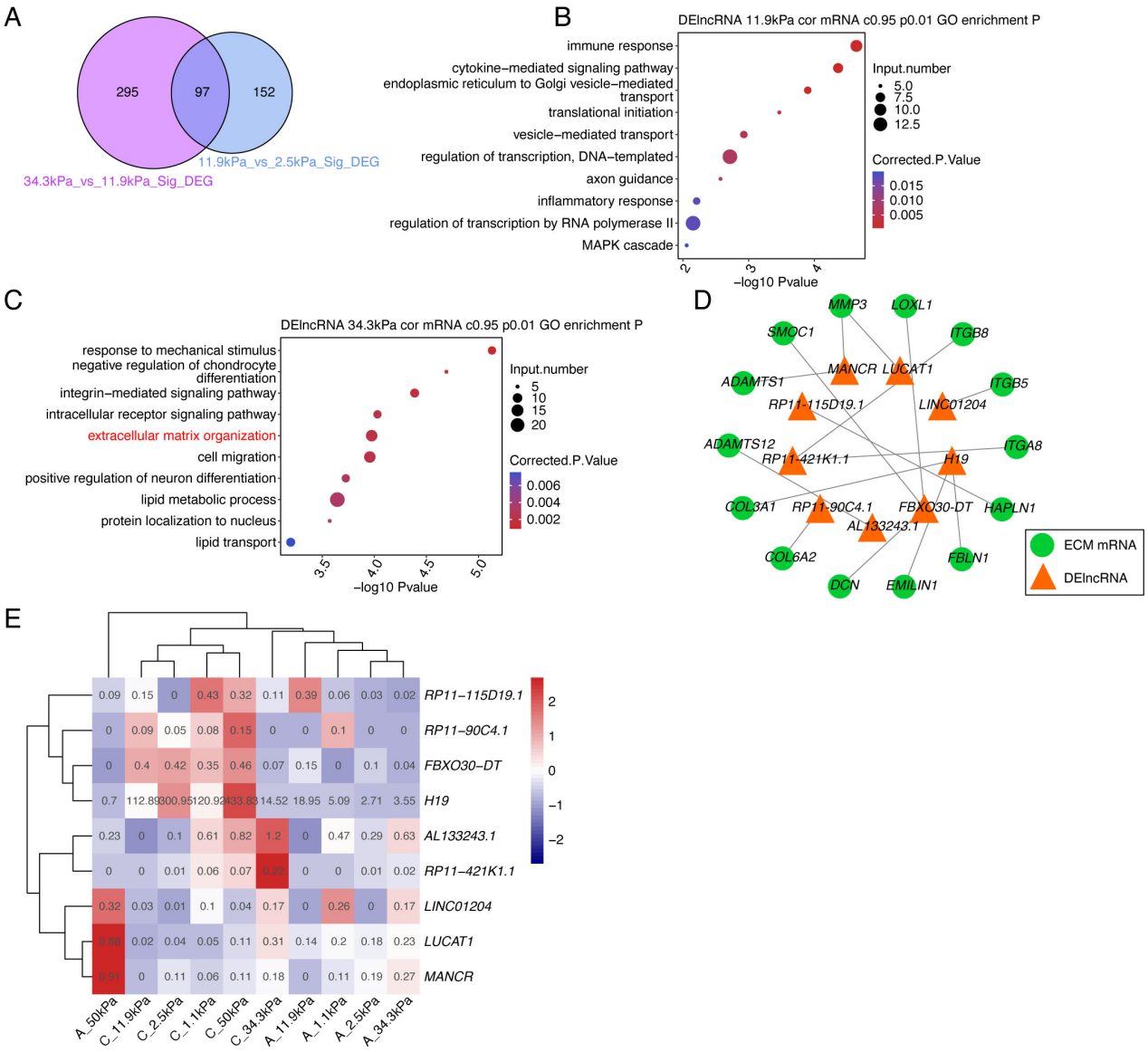

Fig. 2. DElncRs are tightly associated with extracellular matrix (ECM) genes by co-expression analysis. (A) Venn diagram showing the overlapped DElncRs in the 11.9 kPa *vs*. 2.5 kPa and 34.4 kPa *vs*. 11.9 kPa group. (B) Bubble plot showing the top enriched Gene Ontology (GO) Biological Process (BP) pathways of co-expressed DElncRs-DEGs in the 11.9 kPa *vs*. 2.5 kPa group. (C) Bubble plot showing the top enriched GO BP pathways of co-expressed DElncRs-DEGs in the 34.4 kPa *vs*. 11.9 kPa group. (D) Network presentation of DElncR-DEG pairs enriched in ECM-related pathways. (E) Heatmap presentation of DElncRs co-expressed with ECM-related DEGs. DEG, Differentially Expressed Gene.

we investigated the global expression patterns of all ECM-related genes, and found that they were extensively regulated after treatment (Fig. 4H). Finally, we analyzed the overlapped DEGs among these three lncRNAs and found that most of the regulated DEGs were specific (Fig. 4I). We randomly selected three ECM-related genes, including *APOE*, *EMILIN3*, and *F12*, and validated their changed expression levels in SNHG8-OE and NC samples (Fig. 4J). Collectively, these results show that aberrant lncRNA expression can affect the ECM environment, which may contribute to the pathological condition of HTM cells.

3.4 EZH2 Prefers to Bind to Transcripts Enriched in ECM Organization Functions in HTM Cells

LncRNAs regulate their targets in multiple functional types with the help of RNA binding proteins (RBPs), including cis- and trans-acting [42]. A well-studied partner of lncRNAs is EZH2, the core component of the PRC2 complex [43]. We performed CLIP-seq analyses for EZH2 to explore the interacting RNA partners of EZH2 in HTM cells. After alignment of sequenced tags, genomic region distribution analysis showed that compared to IgG, EZH2 preferred to bind to coding sequence (CDS) and 3′UTR regions (Fig. 5A). ABLIRC [35] and CIMS [44] tools were

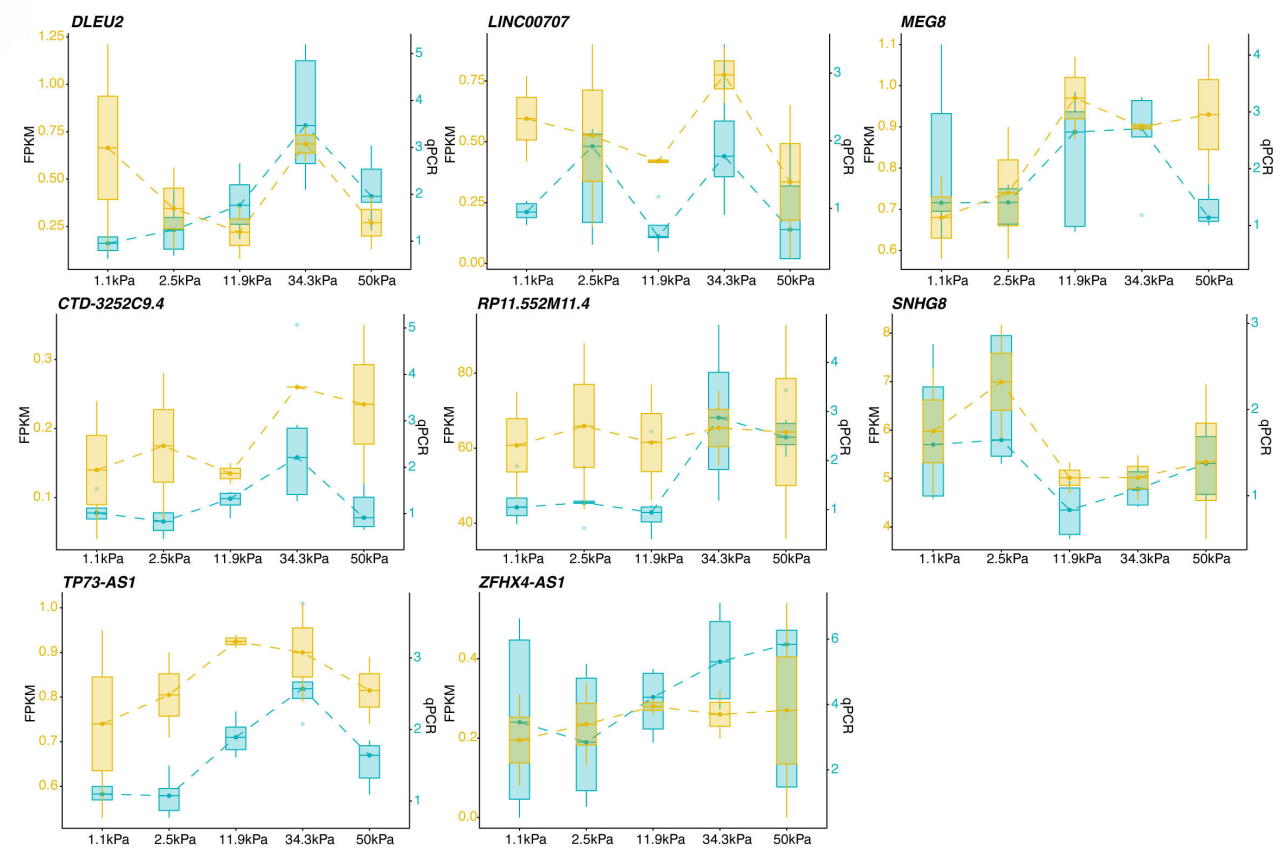

Fig. 3. Reverse Transcription and Quantitative Polymerase Chain Reaction (RT-qPCR) validation of lncRNAs under the effect of substrate stiffness in HTM cells. Box plot showing the RT-qPCR validation of selected lncRNAs for D3 and D5 samples. RNA-seq results (brown box) and RT-qPCR results (light green box) showed the consistency of these two methods. RT-qPCR analysis was performed with three biological replicates.

used to detect EZH2 binding peaks. Several known non-coding RNAs interacting with EZH2 were found to be significantly enriched in EZH2 immunoprecipitation (EZH2-IP) samples compared with IgG control samples (p-value $<$ 0.05), including *XIST* [23] with 3 binding peaks, and *MEG3* [43] with 10 binding peaks (Fig. 5B). We then searched the binding profiles of the above-checked lncRNAs, and found that only *SNHG8* was bound by EZH2 (Fig. 5C). *SNHG8*, a small nucleolar RNA host gene, is known to affect several gastric cancer-specific pathways and the target genes of Epstein–Barr virus (EBV) [45]. The above results showed that *SNHG8* expression levels decreased under higher stiffness (Fig. 3); and that *SNHG8* overexpression could also cause the expression of many ECM-related genes to be dysregulated (Fig. 4D). We analyzed the preferred binding sequences (motifs) of EZH2, and found that AGGUAAG and GAA-repeats were the two most significant motifs for both peak sets (Fig. 5D). We checked the enriched functional pathways of EZH2-bound transcripts in HTM cells. EZH2-bound transcripts identified by CIMS were significantly enriched in axon guidance, gene expression, and ECM organization (Fig. 5E). Overlapping analyses between EZH2-bound transcripts and *SNHG8*-OE-DEGs identified the overlapped genes (Fig. 5F,G). This indicates that *SNHG8* and EZH2 may coordinately regulate the expression of ECM-related genes.

3.5 SNHG8 Promotes ECM Remodeling Gene Expression by Interacting with EZH2 to Decrease the H3K27me3 Marker

The physical interactions between EZH2 and *SNHG8* have been demonstrated, but it remains unclear how this protein-RNA complex plays a role in HTM cells remains unclear. Increasing evidence has shown that EZH2-RNA interactions prevent EZH2 from catalyzing H3K27 methylation to regulate gene expression [46–48]. Thus, we performed ChIP-seq analyses of EZH2 and H3K27me3, with two biological replicates for each. After MACS2 software was used to call peaks [38], significantly enriched binding peaks of EZH2 and H3K27me3 were obtained (p-value $< 1 \times 10^{-5}$) (Fig. 6A). After analyzing the overlapped genes between two biological replicates, 1168 and 4251 genes were found to be bound by EZH2 and H3K27me3, respectively (Fig. 6B,C), with 266 genes being bound by both EZH2 and H3K27me3 (Fig. 6D). Functional enrichment analyses of these genes revealed diverse

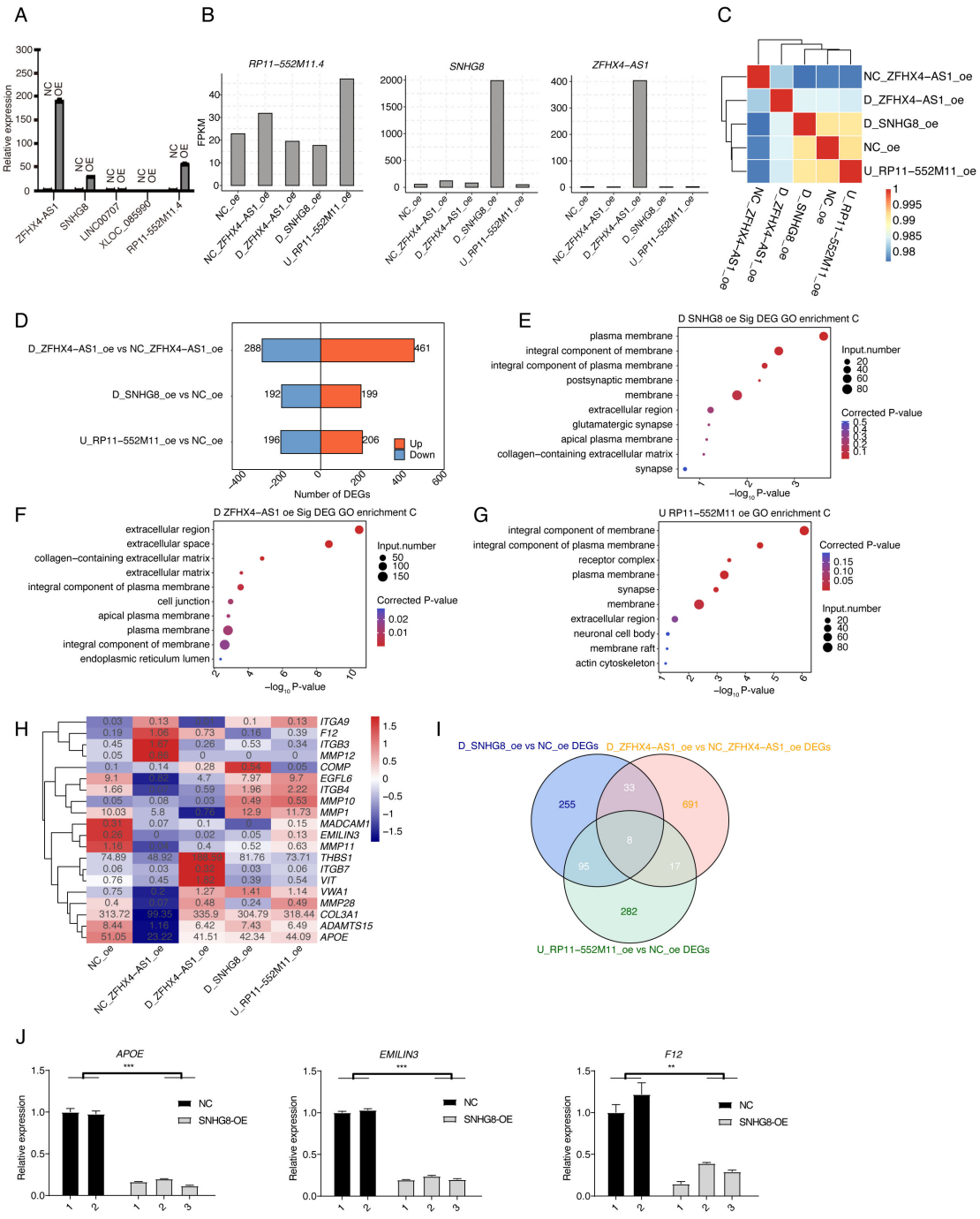

Fig. 4. LncRNA overexpression extensively regulates the expression of ECM remodeling-related genes. (A) Bar plot showing the overexpressed lncRNA levels in HTM cells using RT-qPCR method. (B) Bar plot showing the expression levels of three overexpressed lncRNAs and two negative controls. (C) Sample correlation heatmap of RNA-seq samples. (D) Volcano plot showing the DEGs between overexpressed lncRNAs and negative controls. (E) Bubble plot showing the enriched GO Cellular Component (CC) terms of DEGs from SNHG8-OE samples compared with negative control. (F) The same with (D) but for the DEGs from ZFHX4-AS1-OE. (G) The same with (D) but for the DEGs from RP11-552M11.4-OE. (H) Hierarchical clustering heatmap showing the expression patterns of ECM-associated and ZFHX4-AS1-regulated DEGs. (I) Venn diagram showing the overlapped and specific DEGs among these three DElncRs. (J) Bar plot showing the changed expression levels of APOE, EMILIN3, and F12 between SNHG8-OE *vs.* NC samples using RT-qPCR. One NC sample was removed due to its outlier feature. ** p-value < 0.01; *** p-value < 0.001; Student's t-test. NC, negative control; OE, over expression.

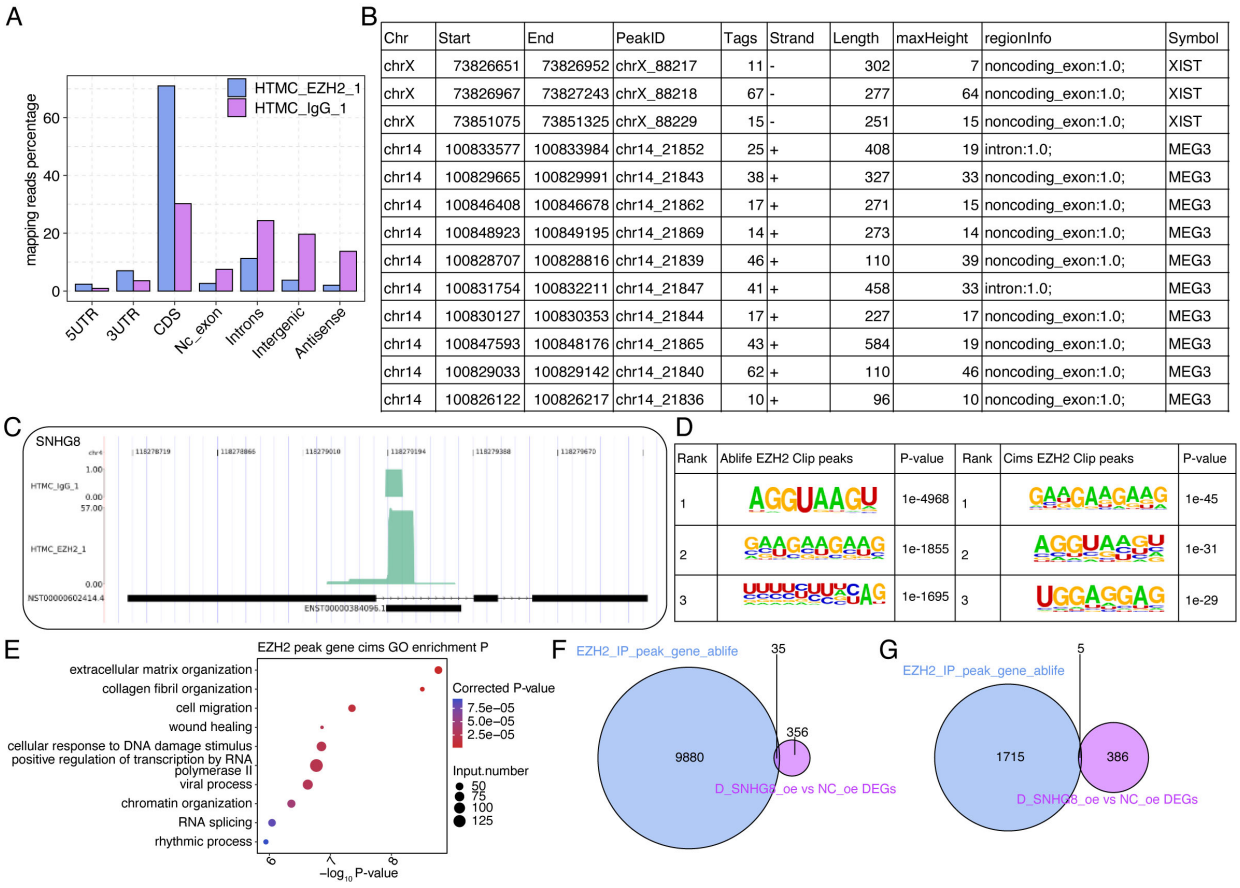

Chr	Start	End	PeakID	Tags	Strand	Length	maxHeight	regionInfo	Symbol
chrX	73826651	73826952	chrX_88217	11	-	302	7	noncoding_exon:1.0;	XIST
chrX	73826967	73827243	chrX_88218	67	-	277	64	noncoding_exon:1.0;	XIST
chrX	73851075	73851325	chrX_88229	15	-	251	15	noncoding_exon:1.0;	XIST
chr14	100833577	100833984	chr14_21852	25	+	408	19	intron:1.0;	MEG3
chr14	100829665	100829991	chr14_21843	38	+	327	33	noncoding_exon:1.0;	MEG3
chr14	100846408	100846678	chr14_21862	17	+	271	15	noncoding_exon:1.0;	MEG3
chr14	100848923	100849195	chr14_21869	14	+	273	14	noncoding_exon:1.0;	MEG3
chr14	100828707	100828816	chr14_21839	46	+	110	39	noncoding_exon:1.0;	MEG3
chr14	100831754	100832211	chr14_21847	41	+	458	33	intron:1.0;	MEG3
chr14	100830127	100830353	chr14_21844	17	+	227	17	noncoding_exon:1.0;	MEG3
chr14	100847593	100848176	chr14_21865	43	+	584	19	noncoding_exon:1.0;	MEG3
chr14	100829033	100829142	chr14_21840	62	+	110	46	noncoding_exon:1.0;	MEG3
chr14	100826122	100826217	chr14_21836	10	+	96	10	noncoding_exon:1.0;	MEG3

Rank	Ablife EZH2 Clip peaks	P-value	Rank	Cims EZH2 Clip peaks	P-value
1		1e-4968	1		1e-45
2		1e-1855	2		1e-31
3		1e-1695	3		1e-29

Fig. 5. EZH2 interacts with mRNAs and lncRNAs in HTM cells. (A) Bar plot showing the genomic distribution of mapped reads in EZH2-IP and IgG samples. (B) Table showing the detailed information of EZH2-bound peaks from XIST and MEG3 lncRNAs using ABLIRC method. (C) Reads density plot for lncRNA SNHG8 in EZH2-IP and IgG samples. (D) Motif analysis showing the top three enriched motifs from EZH2-bound peaks using ABLIRC and CIMS methods. (E) Bubble plot showing the top enriched GO BP pathways of EZH2-bound gene transcripts using CIMS method. (F) Venn diagram showing the overlapped genes between EZH2-bound transcripts (replicate 1) and SNHG8-OE-DEGs. (G) Venn diagram showing the overlapped genes between EZH2-bound transcripts (replicate 2) and SNHG8-OE-DEGs.

functions (Fig. 6E). The *SNHG8*-OE-regulated genes and EZH2- and H3K27me3-bound genes were overlapped to make the functional impacts of the interactions between EZH2 and SNHG8. A total of 49 *SNHG8*-OE-regulated genes were found to be bound by EZH2 or H3K27me3 (Fig. 6F). Functional analyses of these 49 genes showed enriched GO terms extracellular space and extracellular matrix (Fig. 6G), including *HAPLN3*, *TACSTD2*, *COMP*, *TAC1*, *GDF10*, *DLK1*, and *EGF*. These results demonstrate that *SNHG8* and EZH2 could coordinately regulate the expressions of a subset of genes related to ECM-remodeling via the methyltransferase activity of EZH2. However, a large number of DEGs by *SNHG8*-OE were not bound by EZH2 or H3K2me3, indicating that other mechanisms could be involved in the SNHG8-regulated transcriptome in HTM cells, which needs to be further investigated in the future.

4. Discussion

Glaucoma-induced irreversible blindness affected millions of people worldwide. The primary risk factors of glaucoma are increased outflow resistance and elevated IOP mediated by dysregulated TM and ECM [12]. In this study, next generation sequencing and gene interfering technologies were used to explore the transcriptome and epigenetic profiles of altered HTM cells by mimicking the *in vivo* glaucomatous HTM tissue. We focused on the dysregulated lncRNAs and explored their potential functions and targets. Our study revealed that many lncRNAs were dysregulated due to the increased substrate stiffness and that their dysregulation induced the expression changes of genes with important biological functions, including ECM organization and assembly pathways. The identified lncRNA *SNHG8* has potential functions in ECM modulation and may fulfill these functions by interacting with EZH2 or other RNA binding proteins to modulate the transcriptional program of associated genes.

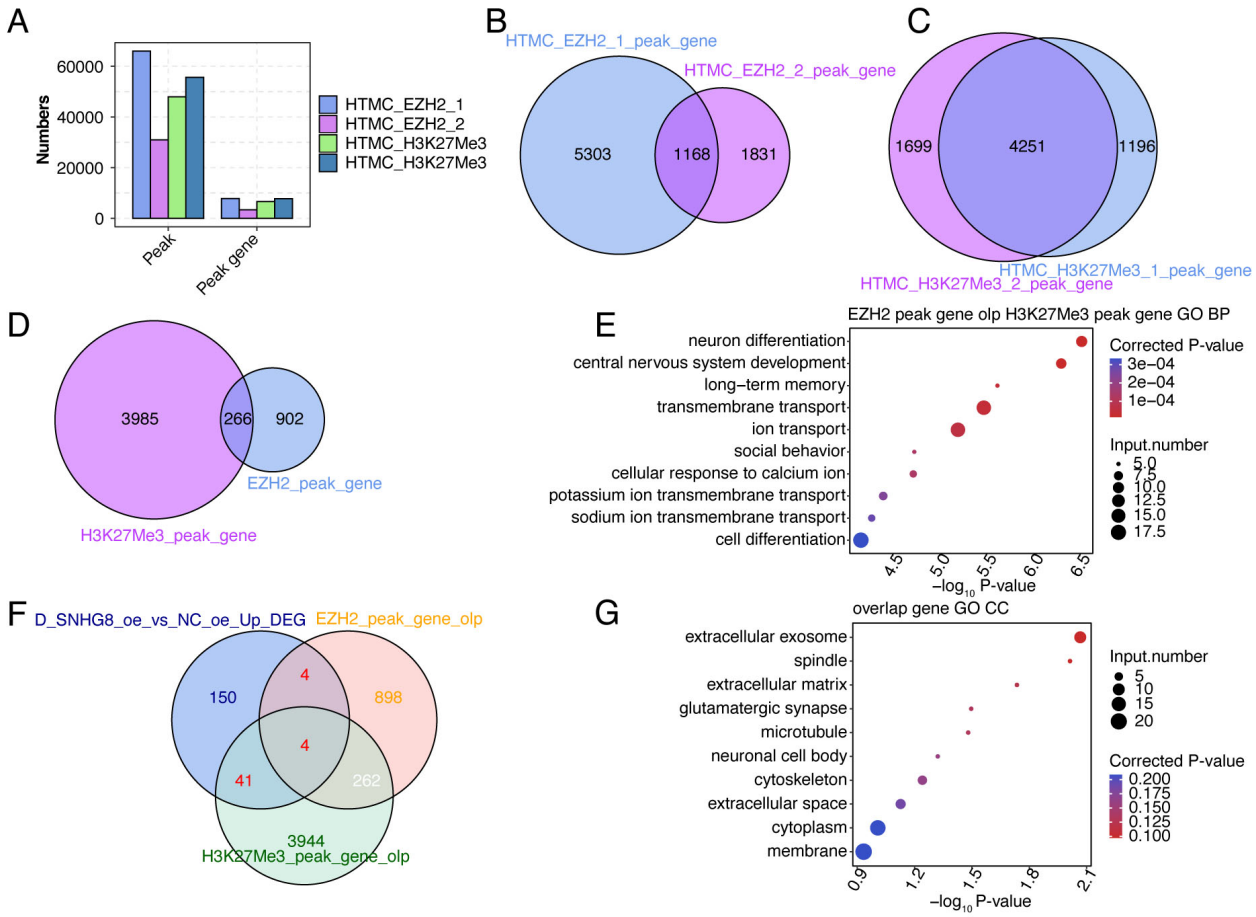

Fig. 6. ChIP-seq analysis reveals the DNA interaction profiles of EZH2 and H3K27me3 in HTM cells. (A) Peaks and genes identified by EZH2 and H3K27me3 ChIP-seq data are shown in the bar plot. (B) Venn diagram showing the overlapped genes between the two replicates of EZH2 ChIP-seq- associated genes. (C) Venn diagram showing the overlapped genes between the two replicates of H3K27me3 ChIP-seq-associated genes. (D) Venn diagram showing the overlapped genes between EZH2 and H3K27me3 ChIP-seq-associated genes. (E) Bubble plot showing the enriched GO BP pathways of overlapped genes in (D). (F) Venn diagram showing the overlapped genes among SNHG8-OE-DEGs, EZH2-associated genes, and H3K27me3-associated genes. (G) Bubble plot showing the enriched GO CC pathways of 49 overlapped genes in (F).

Cells in the HTM tissue play a key role in maintaining IOP homeostasis [49]. A better understanding of this process will greatly improve the therapeutic approaches to glaucoma, a disease whose IOP homeostasis was compromised or lost [50]. Our previous *in vitro* experiment on substrate stiffness-increased HTM cell model revealed the global ECM gene expression changes of HTM cells [15]. The influence of noncoding RNAs on ECM proteins, including several important lncRNAs, has been previously discussed [51]. A total of 248 lncRNAs and 4 hub lncRNAs were identified through competing endogenous RNA network analysis in POAG [52]. Global transcriptome exploration on how HTM cells responded to mechanical stretch also revealed hundreds of dysregulated mRNAs, metabolism- and ECM interaction-associated lncRNAs and several master regulatory microRNAs [53]. Other studies have mainly focused on single lncRNAs and linked them to the genetic basis of glaucoma [18]. In HTM cells, the antisense RNA of TGFβ2, named *TGFβ2-AS1*, could promote ECM production [54]. In this study, hundreds of dysregulated lncRNAs were identified, which are highly correlated with mRNA genes enriched in ECM organization, with most lncRNAs not previously reported to be associated with glaucoma. These results indicate that many lncRNAs involved in transcriptional or post-transcriptional regulation might contribute to the glaucoma phenotypes, suggesting the powerful features of RNA-seq data which could represent a strong substrate to enforce the role of described molecular mechanisms and was validated in recent studies [55–57].

In this study, several lncRNAs were finally identified to modulate ECM gene expression, including *SNHG8*, *ZFHX4-AS1*, and *RP11-552M11.4*. These lncRNAs were mainly analyzed in the tumor area based on searching previous studies. Down-regulation of *ZFHX4-AS1* can suppress the invasion and migration of breast cancer cells via the

Hippo signaling pathway [58], whereas the other functions of *ZFHX4-AS1* still remain largely unknown. In cervical cancer, *RP11-552M11.4* promotes tumorigenesis and development by targeting ATF1 [59], and in ovarian cancer, by targeting BRCA2 [60]. *SNHG8* has many functions, for example, *SNHG8* can regulate EBV-associated gastric cancer [45], and promote the development of hepatocellular carcinoma (HCC) by sponging miR-149-5p [61]. In this study, we investigated how these three lncRNAs transcriptionally regulated ECM genes in HTM cells and found ECM associated genes were extensively regulated by these lnRNAs. Based on the complex functional mechanisms of lncRNAs, we propose that these dysregulated lncRNAs due to substrate stiffness may form a regulatory network with their target molecules to influence the ECM patterns of HTM cells, extending their important regulatory roles and underlying mechanisms in the glaucoma pathogenesis. Meanwhile, due to the lack of solid validation experiments and less biological replicates, further studies should be performed to validate the regulatory mechanisms of these dysregulated lncRNAs.

Furthermore, we found that *SNHG8* could modulate ECM gene expression by interacting with EZH2 through post-transcriptional regulation. A previous study summarized the epigenetic regulatory functions of lncRNAs with the PRC2 complex, which contains the core methyltransferase EZH2 [62]. By interacting with genetic and environmental factors, epigenetic regulation could promote TM fibrosis generation through several pathways, resulting in elevated IOP [63]. A recently published study validated that *SNHG8*, a mechanical force-sensitive lncRNA, can modulate the osteogenic differentiation of periodontal ligament stem cells through epigenetic pathways by regulating EZH2 expression [64]. Another study also reported that *SNHG8* and EZH2 coordinately regulate proliferation and apoptosis in human papillomavirus (HPV)-induced cervical cancer [65]. Using the CLIP-seq data of EZH2, we identified the direct interaction between *SNHG8* and EZH2 in HTM cells. Meanwhile, we also found that EZH2-bound mRNA genes were significantly enriched in ECM-related pathways, which indicated us that *SNHG8* cooperates with EZH2 to regulate the fate of RNAs interacting with them. Meanwhile, we also performed ChIP-seq on EZH2 and H3K27me3 to identify their targeting genes. However, few genes were found to be overlapped between SNHG8-regulated DEGs and genes with both EZH2 and H3K27me3 binding signals, suggesting that the two gene sets function normally without being mutually influenced and other mechanisms may exist for the regulatory program of *SNHG8* in HTM cells.

5. Conclusion

In conclusion, we systematically investigated the lncRNA profiles in HTM cells responding to the increased substrate stiffness and found that the dysregulated lncRNAs were tightly associated with the altered ECM organization, suggesting their important roles in ECM organization and glaucoma pathogenesis. Meanwhile, we explored the direct association between *SNHG8* and EZH2, and discussed how SHNG8 and EZH2 coordinately modulated the expression of the downstream targets. These results provide an understanding of the important roles and molecular functions of lncRNAs in glaucoma progression. The identified lncRNAs, especially SNHG8, and their potential targets could provide potential therapeutic targets in glaucoma treatment in future investigation.

Availability of Data and Materials

The RNA-seq data sets analyzed during the current study are available in the NCBI Gene Expression Omnibus (GEO) repository with ID GSE123100. The other data sets were used under license for the current study and so are not publicly available. Data are however available from the authors upon reasonable request.

Author Contributions

JW and ZY designed the study and revised the manuscript. JG partially designed the study, performed the majority of the experiments, and drafted the manuscript. YW, YS, and DC performed part of the experiments and analyzed the data. YH and XS performed part of the experiments. All authors contributed to editorial changes in the manuscript. All authors read and approved the final manuscript. All authors have participated sufficiently in the work and agreed to be accountable for all aspects of the work.

Ethics Approval and Consent to Participate

Not applicable.

Acknowledgment

Not applicable.

Funding

This work was supported by the National Natural Science Foundation of China (82070961), the Basic Research Project of Shenzhen (JCYJ20230807114605010), Shenzhen Science and Technology Program (No.KCXFZ20230731093359004), and Shenzhen Key Medical Discipline Construction Fund (No. SZXK037).

Conflict of Interest

The authors declare no conflict of interest. Yue Sun, Yunfei Wu, and Dong Chen are employed by Wuhan Ruixing Biotechnology Co., Ltd.

Supplementary Material

Supplementary material associated with this article can be found, in the online version, at https://doi.org/10.31083/j.fbl2903091.

References

[1] Jonas JB, Aung T, Bourne RR, Bron AM, Ritch R, Panda-Jonas S. Glaucoma. Lancet (London, England). 2017; 390: 2183–2193.

[2] Weinreb RN, Leung CKS, Crowston JG, Medeiros FA, Friedman DS, Wiggs JL, *et al*. Primary open-angle glaucoma. Nature Reviews. Disease Primers. 2016; 2: 16067.

[3] Matlach J, Bender S, König J, Binder H, Pfeiffer N, Hoffmann EM. Investigation of intraocular pressure fluctuation as a risk factor of glaucoma progression. Clinical Ophthalmology (Auckland, N.Z.). 2018; 13: 9–16.

[4] Kim JH, Caprioli J. Intraocular Pressure Fluctuation: Is It Important? Journal of Ophthalmic & Vision Research. 2018; 13: 170–174.

[5] Roberts AL, Mavlyutov TA, Perlmutter TE, Curry SM, Harris SL, Chauhan AK, *et al*. Fibronectin extra domain A (FN-EDA) elevates intraocular pressure through Toll-like receptor 4 signaling. Scientific Reports. 2020; 10: 9815.

[6] Tsukamoto T, Kajiwara K, Nada S, Okada M. Src mediates TGF-β-induced intraocular pressure elevation in glaucoma. Journal of Cellular Physiology. 2019; 234: 1730–1744.

[7] Stamer WD, Lei Y, Boussommier-Calleja A, Overby DR, Ethier CR. eNOS, a pressure-dependent regulator of intraocular pressure. Investigative Ophthalmology & Visual Science. 2011; 52: 9438–9444.

[8] Stamer WD, Clark AF. The many faces of the trabecular meshwork cell. Experimental Eye Research. 2017; 158: 112–123.

[9] Gonzalez JM, Jr, Hamm-Alvarez S, Tan JCH. Analyzing live cellularity in the human trabecular meshwork. Investigative Ophthalmology & Visual Science. 2013; 54: 1039–1047.

[10] Vranka JA, Kelley MJ, Acott TS, Keller KE. Extracellular matrix in the trabecular meshwork: intraocular pressure regulation and dysregulation in glaucoma. Experimental Eye Research. 2015; 133: 112–125.

[11] Acott TS, Kelley MJ. Extracellular matrix in the trabecular meshwork. Experimental Eye Research. 2008; 86: 543–561.

[12] Keller KE, Peters DM. Pathogenesis of glaucoma: Extracellular matrix dysfunction in the trabecular meshwork-A review. Clinical & Experimental Ophthalmology. 2022; 50: 163–182.

[13] Wood JA, McKee CT, Thomasy SM, Fischer ME, Shah NM, Murphy CJ, *et al*. Substratum compliance regulates human trabecular meshwork cell behaviors and response to latrunculin B. Investigative Ophthalmology & Visual Science. 2011; 52: 9298–9303.

[14] McKee CT, Wood JA, Shah NM, Fischer ME, Reilly CM, Murphy CJ, *et al*. The effect of biophysical attributes of the ocular trabecular meshwork associated with glaucoma on the cell response to therapeutic agents. Biomaterials. 2011; 32: 2417–2423.

[15] Tie J, Chen D, Guo J, Liao S, Luo X, Zhang Y, *et al*. Transcriptome-wide study of the response of human trabecular meshwork cells to the substrate stiffness increase. Journal of Cellular Biochemistry. 2020; 121: 3112–3123.

[16] Shen W, Han Y, Huang B, Qi Y, Xu L, Guo R, *et al*. MicroRNA-483-3p Inhibits Extracellular Matrix Production by Targeting Smad4 in Human Trabecular Meshwork Cells. Investigative Ophthalmology & Visual Science. 2015; 56: 8419–8427.

[17] Lauwen S, de Jong EK, Lefeber DJ, den Hollander A. Omics Biomarkers in Ophthalmology. Investigative Ophthalmology & Visual Science. 2017; 58: BIO88–BIO98.

[18] Cissé Y, Bai L, Meng T. LncRNAs in genetic basis of glaucoma. BMJ Open Ophthalmology. 2018; 3: e000131.

[19] Johnson WM, Finnegan LK, Hauser MA, Stamer WD. lncRNAs, DNA Methylation, and the Pathobiology of Exfoliation Glaucoma. Journal of Glaucoma. 2018; 27: 202–209.

[20] Yao J, Wang XQ, Li YJ, Shan K, Yang H, Wang YN, *et al.* Long non-coding RNA MALAT1 regulates retinal neurodegeneration through CREB signaling. EMBO molecular medicine. 2016; 8: 346–362.

[21] Wan P, Su W, Zhuo Y. The Role of Long Noncoding RNAs in Neurodegenerative Diseases. Molecular Neurobiology. 2017; 54: 2012–2021.

[22] McHugh CA, Chen CK, Chow A, Surka CF, Tran C, McDonel P, *et al*. The Xist lncRNA interacts directly with SHARP to silence transcription through HDAC3. Nature. 2015; 521: 232–236.

[23] Engreitz JM, Pandya-Jones A, McDonel P, Shishkin A, Sirokman K, Surka C, *et al*. The Xist lncRNA exploits three-dimensional genome architecture to spread across the X chromosome. Science (New York, N.Y.). 2013; 341: 1237973.

[24] Overby DR, Zhou EH, Vargas-Pinto R, Pedrigi RM, Fuchshofer R, Braakman ST, *et al*. Altered mechanobiology of Schlemm's canal endothelial cells in glaucoma. Proceedings of the National Academy of Sciences of the United States of America. 2014; 111: 13876–13881.

[25] Livak KJ, Schmittgen TD. Analysis of relative gene expression data using real-time quantitative PCR and the 2(-Delta Delta C(T)) Method. Methods (San Diego, Calif.). 2001; 25: 402–408.

[26] Kim D, Langmead B, Salzberg SL. HISAT: a fast spliced aligner with low memory requirements. Nature Methods. 2015; 12: 357–360.

[27] Trapnell C, Williams BA, Pertea G, Mortazavi A, Kwan G, van Baren MJ, *et al*. Transcript assembly and quantification by RNA-Seq reveals unannotated transcripts and isoform switching during cell differentiation. Nature Biotechnology. 2010; 28: 511–515.

[28] Kovaka S, Zimin AV, Pertea GM, Razaghi R, Salzberg SL, Pertea M. Transcriptome assembly from long-read RNA-seq alignments with StringTie2. Genome Biology. 2019; 20: 278.

[29] Kong L, Zhang Y, Ye ZQ, Liu XQ, Zhao SQ, Wei L, *et al*. CPC: assess the protein-coding potential of transcripts using sequence features and support vector machine. Nucleic Acids Research. 2007; 35: W345–W349.

[30] Wang G, Yin H, Li B, Yu C, Wang F, Xu X, *et al*. Characterization and identification of long non-coding RNAs based on feature relationship. Bioinformatics (Oxford, England). 2019; 35: 2949–2956.

[31] Sun L, Luo H, Bu D, Zhao G, Yu K, Zhang C, *et al*. Utilizing sequence intrinsic composition to classify protein-coding and long non-coding transcripts. Nucleic Acids Research. 2013; 41: e166.

[32] Wang L, Park HJ, Dasari S, Wang S, Kocher JP, Li W. CPAT: Coding-Potential Assessment Tool using an alignment-free logistic regression model. Nucleic Acids Research. 2013; 41: e74.

[33] Wu S, Cheng C, Zhu W, Yang J, He BB, Li S, *et al*. Whole transcriptome analysis reveals that immune infiltration- lncRNAs are related to cellular apoptosis in liver transplantation. Frontiers in Immunology. 2023; 14: 1152742.

[34] Robinson MD, McCarthy DJ, Smyth GK. edgeR: a Bioconductor package for differential expression analysis of digital gene expression data. Bioinformatics (Oxford, England). 2010; 26: 139–140.

[35] Xia H, Chen D, Wu Q, Wu G, Zhou Y, Zhang Y, *et al*. CELF1 preferentially binds to exon-intron boundary and regulates alternative splicing in HeLa cells. Biochimica et Biophysica Acta. Gene Regulatory Mechanisms. 2017; 1860: 911–921.

[36] Zhang C, Darnell RB. Mapping in vivo protein-RNA interactions at single-nucleotide resolution from HITS-CLIP data. Nat Biotechnol. 2011; 29: 607–614.

[37] Langmead B, Salzberg SL. Fast gapped-read alignment with Bowtie 2. Nature Methods. 2012; 9: 357–359.

[38] Zhang Y, Liu T, Meyer CA, Eeckhoute J, Johnson DS, Bernstein BE, *et al*. Model-based analysis of ChIP-Seq (MACS). Genome Biology. 2008; 9: R137.

[39] Heinz S, Benner C, Spann N, Bertolino E, Lin YC, Laslo P, *et al*. Simple combinations of lineage-determining transcription factors prime cis-regulatory elements required for macrophage and B cell identities. Molecular Cell. 2010; 38: 576–589.
[40] Xie C, Mao X, Huang J, Ding Y, Wu J, Dong S, *et al*. KOBAS 2.0: a web server for annotation and identification of enriched pathways and diseases. Nucleic Acids Research. 2011; 39: W316–W322.
[41] Last JA, Pan T, Ding Y, Reilly CM, Keller K, Acott TS, *et al*. Elastic modulus determination of normal and glaucomatous human trabecular meshwork. Investigative Ophthalmology & Visual Science. 2011; 52: 2147–2152.
[42] Guttman M, Rinn JL. Modular regulatory principles of large non-coding RNAs. Nature. 2012; 482: 339–346.
[43] Kaneko S, Bonasio R, Saldaña-Meyer R, Yoshida T, Son J, Nishino K, *et al*. Interactions between JARID2 and noncoding RNAs regulate PRC2 recruitment to chromatin. Molecular Cell. 2014; 53: 290–300.
[44] Zhang C, Darnell RB. Mapping in vivo protein-RNA interactions at single-nucleotide resolution from HITS-CLIP data. Nature Biotechnology. 2011; 29: 607–614.
[45] Huang T, Ji Y, Hu D, Chen B, Zhang H, Li C, *et al*. SNHG8 is identified as a key regulator of epstein-barr virus(EBV)-associated gastric cancer by an integrative analysis of lncRNA and mRNA expression. Oncotarget. 2016; 7: 80990–81002.
[46] Kaneko S, Son J, Shen SS, Reinberg D, Bonasio R. PRC2 binds active promoters and contacts nascent RNAs in embryonic stem cells. Nature Structural & Molecular Biology. 2013; 20: 1258–1264.
[47] Beltran M, Yates CM, Skalska L, Dawson M, Reis FP, Viiri K, *et al*. The interaction of PRC2 with RNA or chromatin is mutually antagonistic. Genome Research. 2016; 26: 896–907.
[48] Sui B, Chen D, Liu W, Wu Q, Tian B, Li Y, *et al*. A novel antiviral lncRNA, EDAL, shields a T309 O-GlcNAcylation site to promote EZH2 lysosomal degradation. Genome Biology. 2020; 21: 228.
[49] Clark AF. The cell and molecular biology of glaucoma: biomechanical factors in glaucoma. Investigative Ophthalmology & Visual Science. 2012; 53: 2473–2475.
[50] Johnstone MA. Intraocular pressure regulation: findings of pulse-dependent trabecular meshwork motion lead to unifying concepts of intraocular pressure homeostasis. Journal of Ocular Pharmacology and Therapeutics: the Official Journal of the Association for Ocular Pharmacology and Therapeutics. 2014; 30: 88–93.
[51] Akbari Dilmaghnai N, Shoorei H, Sharifi G, Mohaqiq M, Majidpoor J, Dinger ME, *et al*. Non-coding RNAs modulate function of extracellular matrix proteins. Biomedicine & Pharmacotherapy = Biomedecine & Pharmacotherapie. 2021; 136: 111240.
[52] Zhou M, Lu B, Tan W, Fu M. Identification of lncRNA-miRNA-mRNA regulatory network associated with primary open angle glaucoma. BMC Ophthalmology. 2020; 20: 104.
[53] Youngblood H, Cai J, Drewry MD, Helwa I, Hu E, Liu S, *et al*. Expression of mRNAs, miRNAs, and lncRNAs in Human Trabecular Meshwork Cells Upon Mechanical Stretch. Investigative Ophthalmology & Visual Science. 2020; 61: 2.
[54] Lv Y, Zhang Z, Xing X, Liu A. lncRNA TGFβ2-AS1 promotes ECM production via TGF-β2 in human trabecular meshwork cells. Biochemical and Biophysical Research Communications. 2020; 527: 881–888.
[55] Scimone C, Donato L, Alafaci C, Granata F, Rinaldi C, Longo M, *et al*. High-Throughput Sequencing to Detect Novel Likely Gene-Disrupting Variants in Pathogenesis of Sporadic Brain Arteriovenous Malformations. Frontiers in Genetics. 2020; 11: 146.
[56] Scimone C, Bramanti P, Ruggeri A, Donato L, Alafaci C, Crisafulli C, *et al*. CCM3/SERPINI1 bidirectional promoter variants in patients with cerebral cavernous malformations: a molecular and functional study. BMC Medical Genetics. 2016; 17: 74.
[57] Scimone C, Bramanti P, Ruggeri A, Katsarou Z, Donato L, Sidoti A, *et al*. Detection of Novel Mutation in Ccm3 Causes Familial Cerebral Cavernous Malformations. Journal of Molecular Neuroscience: MN. 2015; 57: 400–403.
[58] Li SY, Wang H, Mai HF, Li GF, Chen SJ, Li GS, *et al*. Down-regulated long non-coding RNA RNAZFHX4-AS1 suppresses invasion and migration of breast cancer cells via FAT4-dependent Hippo signaling pathway. Cancer Gene Therapy. 2019; 26: 374–387.
[59] Xu Y, Zhou W, Zhang C, Liu X, Lv J, Li X, *et al*. Long non-coding RNA RP11-552M11.4 favors tumorigenesis and development of cervical cancer via modulating miR-3941/ATF1 signaling. International Journal of Biological Macromolecules. 2019; 130: 24–33.
[60] Huang K, Geng J, Wang J. Long non-coding RNA RP11-552M11.4 promotes cells proliferation, migration and invasion by targeting BRCA2 in ovarian cancer. Cancer Science. 2018; 109: 1428–1446.
[61] Dong J, Teng F, Guo W, Yang J, Ding G, Fu Z. lncRNA SNHG8 Promotes the Tumorigenesis and Metastasis by Sponging miR-149-5p and Predicts Tumor Recurrence in Hepatocellular Carcinoma. Cellular Physiology and Biochemistry: International Journal of Experimental Cellular Physiology, Biochemistry, and Pharmacology. 2018; 51: 2262–2274.
[62] Lee JT. Epigenetic regulation by long noncoding RNAs. Science (New York, N.Y.). 2012; 338: 1435–1439.
[63] Gauthier AC, Liu J. Epigenetics and Signaling Pathways in Glaucoma. BioMed Research International. 2017; 2017: 5712341.
[64] Zhang Z, He Q, Yang S, Zhao X, Li X, Wei F. Mechanical force-sensitive lncRNA SNHG8 inhibits osteogenic differentiation by regulating EZH2 in hPDLSCs. Cellular Signalling. 2022; 93: 110285.
[65] Qu X, Li Y, Wang L, Yuan N, Ma M, Chen Y. LncRNA SNHG8 accelerates proliferation and inhibits apoptosis in HPV-induced cervical cancer through recruiting EZH2 to epigenetically silence RECK expression. Journal of Cellular Biochemistry. 2020; 121: 4120–4129.